Journal of Alloys and Compounds 509 (2011) 8901–8906

Contents lists available at ScienceDirect

Journal of Alloys and Compounds

journal homepage: www.elsevier.com/locate/jallcom

Dielectric properties of iron doped calcium copper titanate, $CaCu_{2.9}Fe_{0.1}Ti_4O_{12}$

Alok Kumar Rai[a], Nitish Kumar Singh[c], Sang-Kwon Lee[a], K.D. Mandal[b], D. Kumar[c], Om Parkash[c,*]

[a] Department of Semiconductor Science and Technology, SPRC, Chonbuk National University, Jeonju 561-756, Republic of Korea
[b] Department of Applied Chemistry, Institute of Technology, Banaras Hindu University, Varanasi 221005, U.P., India
[c] Department of Ceramic Engineering, Institute of Technology, Banaras Hindu University, Varanasi 221005, U.P., India

ARTICLE INFO

Article history:
Received 21 November 2010
Received in revised form 1 June 2011
Accepted 6 June 2011
Available online 20 July 2011

Keywords:
Ceramics
Chemical synthesis
Dielectric response
Grain boundaries
X-ray diffraction

ABSTRACT

$CaCu_{2.9}Fe_{0.1}Ti_4O_{12}$ (CCFTO) has been prepared by a novel semi-wet route and its dielectric properties have been studied in the temperature range 300–500 K. It is found that dielectric constant (ε) decreases drastically in the frequency range 100 Hz to 1 MHz. Complex plane impedance and modulus analysis was done to understand this drastic decrease in ε. Oxidation state of various ions was studied using X-ray photoelectron spectroscopy (XPS). The decrease in the permittivity of CCFTO can be attributed to two factors: the suppression of the Ca/Cu disorder in CCFTO which is observed in $CaCu_3Ti_4O_{12}$ (CCTO) and the absence of the grain boundary internal barrier layer capacitance mechanism.

1. Introduction

$CaCu_3Ti_4O_{12}$ (CCTO) which belongs to a family of compounds of the type $ACu_3Ti_4O_{12}$ was discovered in 1967 [1]. It has been studied extensively due to its very high dielectric constant (ε) viz. $\sim 10^5$ which remains almost frequency independent up to 10^6 Hz. It is also temperature independent in the temperature range 100–600 K [2,3]. Attempts have been made to understand the origin of this giant dielectric constant. It has been reported that TiO_2 and $ATiO_3$ perovskite oxides (where A = Ca, Sr, and Ba) lose small amount of oxygen during sintering at high temperature. On cooling from the sintering temperature, re-oxidation takes place. Re-oxidation occurs only at the surface layers and grain boundaries due to rapidly falling temperature and short time available during cooling. This leads to the formation of insulating layers at surface and grain boundaries. The bulk material remains semiconducting. This produces barrier layers at interfaces [4,5]. A vary large value of dielectric constant of CCTO has been explained on the basis of this internal boundary layers capacitance (IBLC) model [6]. Zhu et al. [7] observed the disorder at Ca/Cu sites in single crystal CCTO based on integrated study using quantitative electron diffraction and extended X-ray absorption fine structure. They attributed the giant permittivity to this kind of Ca/Cu disorder.

CCTO also exhibits high dielectric loss. This limits its use in devices. Perovskite structure is flexible i.e. its properties can be tailored by modifying the chemical compositions through a variety of possible substitutions [8,9]. It has been reported that doping 2 at.% Fe at Ti site in CCTO leads to a drastic decrease in the value of its dielectric constant [10]. Substitution of Mn on Cu as well as Ti site has also been reported to reduce the dielectric constant drastically [11,12]. This has been explained on the basis of suppression of barrier layers formation at grain boundaries. Substitution of Sn on Ti site has been reported to reduce dielectric constant as well as dielectric loss [13]. This enhances the non-ohmic character of CCTO. Doping of Pr on Ca site also suppresses the dielectric constant as well as dielectric loss of CCTO [14]. Dielectric loss is reduced significantly without affecting the high value of dielectric constant (>15,000) on substituting 2 mol% of cesium (Cs) on Ca site [15]. In the present investigation, an effort has been made to substitute Fe on Cu site in CCTO and study its dielectric properties. Materials based on CCTO are synthesized by conventional solid state method and using various chemical routes [16,17]. Solid state ceramic method requires repeated calcination and sintering at high temperature ($\sim$1000 °C). Chemical routes such as sol–gel and co-precipitation methods require very expensive raw materials e.g. metal alkoxides, titanium tetrachloride, etc. In the present work, an effort has been made to prepare $CaCu_{2.9}Fe_{0.1}Ti_4O_{12}$ (CCFTO) by a novel semi-wet route at relatively low temperature [18,19]. This novel route employs citrate–nitrate gel chemical method using TiO_2 in place of very expensive titanium compounds mentioned above. Characterization of the sample is done using powder X-ray diffraction (XRD), scanning electron microscopy (SEM), X-ray photoelectron spectroscopy (XPS) and by measurement of dielectric properties and impedance analysis.

* Corresponding author. Tel.: +91 0542 2307042/2307043; fax: +91 542 2368428.
E-mail address: oprakash.cer@itbhu.ac.in (O. Parkash).

0925-8388/$ – see front matter © 2011 Elsevier B.V. All rights reserved.
doi:10.1016/j.jallcom.2011.06.008

2. Experimental

$Ca(NO_3)_2{\cdot}4H_2O$ (99.5%, Qualigens, India), $Cu(NO_3)_2{\cdot}3H_2O$ (99.5%, Merck, India), $Fe(NO_3)_3{\cdot}9H_2O$ (99.8%, Merck, India), TiO_2 (99.5%, Merck, India) and citric acid (99.5%, Merck, India) were used as raw materials. One molar solution of calcium nitrate, copper nitrate and ferric nitrate was prepared. Appropriate amount of solid TiO_2 powder was added to the mixed solutions so that ratio of concentration of Ca:Cu:Fe:Ti is 1:2.9:0.1:4 in the resulting mixture. Citric acid (equivalent to metal ions) was then added to this solution. The solution was evaporated on a hot plate at 70–80 °C with constant stirring followed by drying in an oven at 100–120 °C overnight to get the dry gel. The dried CCFTO gel was calcined in air at 800 °C for 6 h. The calcined powder was pressed into cylindrical pellets (dia ~ 12 mm and thickness ~ 1–2 mm) uniaxially using a hydraulic press. The pressed samples were sintered at 900 °C for 6 h in air. Heating as well as cooling rate of 5 °C/min was used during calcination and sintering.

XRD patterns of the calcined and sintered powder were recorded using Rich-Seifert, ID-3000 diffractometer operated at 40 kV and 30 mA employing Cu-Kα radiation (λ = 1.540598 Å). Microstructure and chemical composition of the sample was studied using freshly fractured surface of the sintered sample by Hitache scanning electron microscope (SEM) (model: S-4800) equipped with energy dispersive X-ray (EDX) spectrometer operated at 15 kV. Dielectric measurements were made using a pellet, both surfaces of which were polished and coated with silver paint. An impedance analyzer (Novocontrol Alpha-A High Performance Frequency Analyzer) was used to measure the capacitance, resistance and dielectric loss in the temperature and frequency range of 300–500 K and 10^2–10^6 Hz, respectively. Complex plane impedance and modulus plots were also recorded by this analyzer. X-ray photoelectron spectra (XPS) were recorded using AXIS-NOVA (Kratos Inc.) having a monochromatic Al-Kα X-ray source (1486.6 eV). Kinetic energies of the photoelectrons of interest were measured using a hemispherical electron analyzer operating in the constant pass energy mode. The base pressure along the analysis was maintained at 4.2×10^{-9} Torr. Before analysis, the samples were cleaned by ion-bombardment using an Ar^+ beam (2 kV) for 2 min. X-ray photoelectron spectra (XPS) data were signal averaged and taken at an increment of 0.05 eV with dwelling times of 100 ms. Binding energies were calibrated relative to the C 1s peak at 284.6 eV from the residual carbon contamination of the samples. High-resolution spectral envelopes were obtained by curve fitting synthetic peak components using the software package 'XPS Peak'.

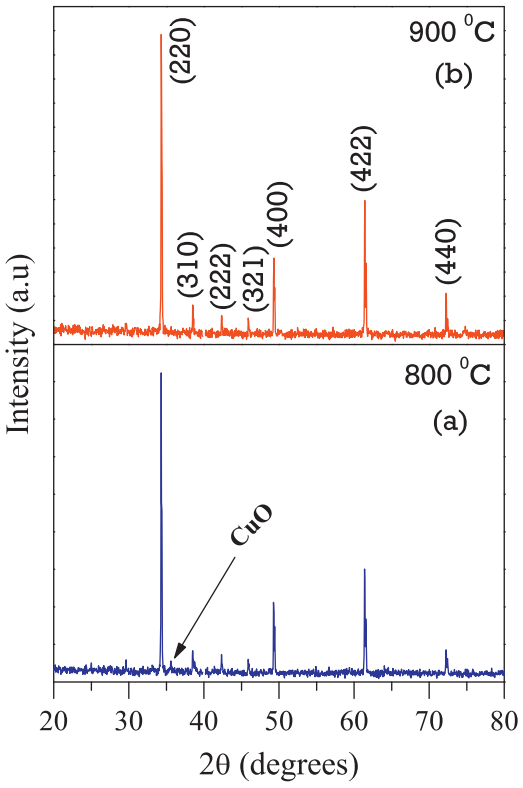

Fig. 1. X-ray powder diffraction patterns for the system $CaCu_{2.9}Fe_{0.1}Ti_4O_{12}$ (CCFTO). (a) Calcined at 800 °C for 6 h and (b) sintered at 900 °C for 6 h.

3. Results and discussion

Fig. 1(a and b) shows XRD patterns of CCFTO powder obtained by calcination of gel at 800 °C and sintering of calcined powder at 900 °C, respectively. XRD pattern of the powder calcined at 800 °C (Fig. 1(a)) shows the presence of CuO phase. XRD pattern of the sample sintered at 900 °C shows the formation of solid solution. This shows that the sample can be prepared by the present process at much lower temperature than the solid state ceramic method. XRD data were indexed on the basis of JCPDS, card no. 75-2188 of CCTO. CCFTO has a cubic structure with lattice parameter '*a*' = 7.379 ± 0.001 Å. This is slightly less than the lattice parameter of CCTO reported previously [20]. The change of lattice parameter is due to the difference between the ionic radius of the host (Cu^{2+}) and substituted ion (Fe^{3+}).

Fig. 2(a–c) shows scanning electron micrograph (SEM), EDX image and EDX spectrum of fractured surface of CCFTO, respectively. A dense but inhomogeneous microstructure consisting of a few large grains and mostly small grains is observed. Small grains have size in the range 1–5 μm. The large grains are separated from one another by regions consisting of fine grains. Fig. 2(b) shows the EDX spectrum of the region containing both large as well as small grains of CCFTO ceramic. Ca, Cu, Ti, Fe and O are found to be 6.45, 29.23, 30.86, 0.95 and 32.51% by weight, respectively. This is consistent with the stoichiometry of CCFTO within the experimental error. A spurious signal was found for presence of platinum (Pt) due to platinum paint coated on the sample.

Temperature dependence of dielectric constant (ε) and dielectric loss (tan δ) of CCFTO at a few selected frequencies between 100 Hz and 100 kHz is shown in Fig. 3(a and b), respectively. Initially a plateau is observed near room temperature. This is followed by a rapid increase over a range of temperature. Another plateau appears after this. It is again followed by a region exhibiting a sharp increase in ε with temperature. This sharp increase is due to rapid increase in the space charge polarization. Space charge polarization is present because of chemical microheterogeneities. Microheterogeneities arise due to random occupation of equivalent crystallographic sites (square planer) by Cu^{2+} and Fe^{3+} ions. Difference in the chemical composition between these microregions leads to difference between conductivity of these regions. This gives rise to space charge polarisation. The conductivity increases exponentially with temperature. Therefore, the difference between conductivity will also increase rapidly. This leads to a rapid increase in the dielectric constant at high temperature. It seems that this difference increases rapidly beyond the temperature where the second plateau ends. The transition temperature between any two regions shifts to higher temperature side with increasing frequency of measurement. This behavior is similar to that of relaxors [21].

Peaks are also observed in tan δ vs. T plots corresponding to the inflexion point in the ε vs. T plots (Fig. 3(b)). It is observed that the position of the peak shifts to higher temperature with increasing frequency. Variation of ε and tan δ with frequency at a few temperatures, shown in Fig. 4(a and b), also indicates the presence of a dielectric relaxation. This figure shows that there is a large difference in the temperature (~20–25 °C) between the point of inflexion in ε vs. T plot (Fig. 3(a)) and peak temperature in tan δ vs. T plot (Fig. 3(b)). This shows that this relaxation is due to Maxwell–Wagner polarisation [22]. Had it been Debye type relaxation, the inflexion point in Fig. 3(a) and peak in Fig. 3(b) would have appeared at the same temperature.

Impedance and modulus analysis separates the contributions of the grains, grain boundaries and electrode specimen interface to the total observed resistance and capacitance of the sample, respectively [23]. Typical complex plane impedance plot obtained for CCFTO at 400 K is shown in Fig. 5. Similar plots are observed at other temperatures (350 K and 450 K). Two arcs are clearly observed in these plots. The intercept of the arc, in the higher frequency range, passing through the origin on Z' axis gives the contribution of the

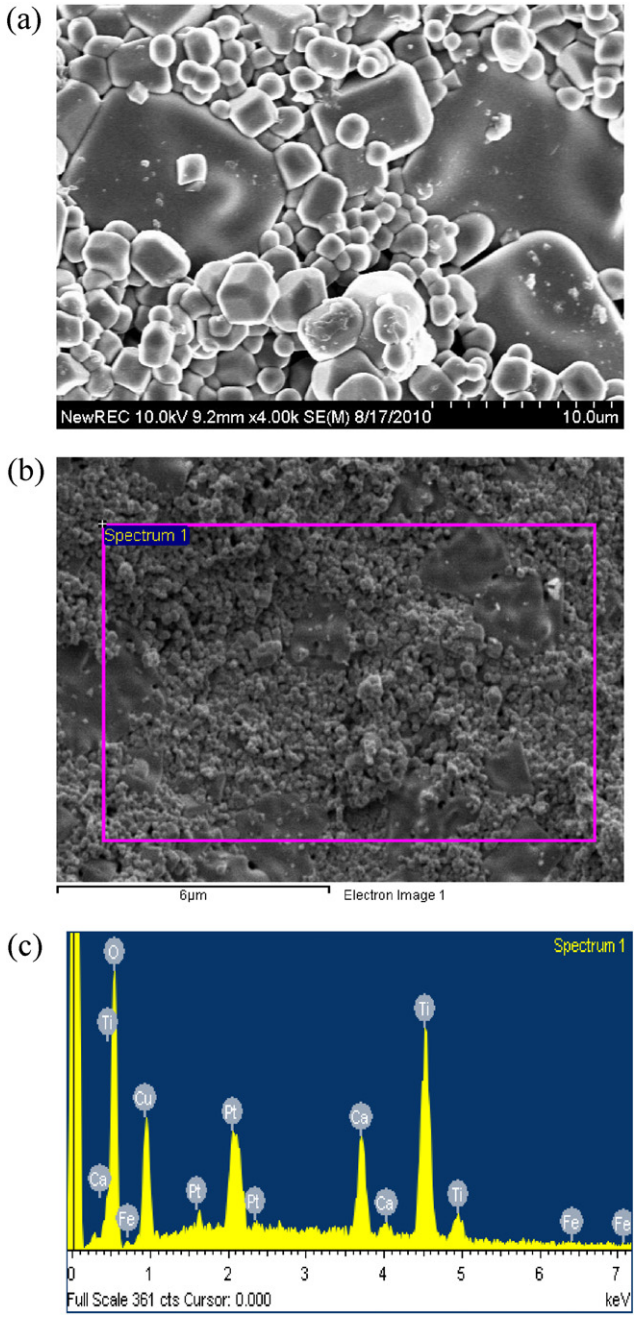

Fig. 2. (a) SEM micrographs, (b) EDX image and (c) EDX spectra of $CaCu_{2.9}Fe_{0.1}Ti_4O_{12}$. (CCFTO). Pt signal comes from coating.

resistance, R_g, of the grains to the total observed resistance. Another arc in the lower frequency range gives contribution of the resistance, R_{gb}, of the grain boundaries to the total observed resistance. Values of corresponding capacitance C_g and C_{gb} can be obtained from the relation: $\omega RC = 1$ where ω is the angular frequency at the peak of circular arc and $\omega = 2\pi f$, f being the frequency in Hz. The value of resistance obtained for grains (R_g) is $3.9 \times 10^5\ \Omega$ while that of grain boundaries is $5.79 \times 10^5\ \Omega$ at 400 K. This shows that the grains as well as grain boundaries are insulating. This leads to suppression of formation of IBLC layers resulting in very low value of dielectric constant.

Modulus spectroscopic plots of CCFTO at a few temperatures are shown in Fig. 6(a). These plots can be resolved into two Gaussian curves as shown in Fig. 6(b) indicating the presence of two relaxation processes. Relaxation time, τ is determined from the higher

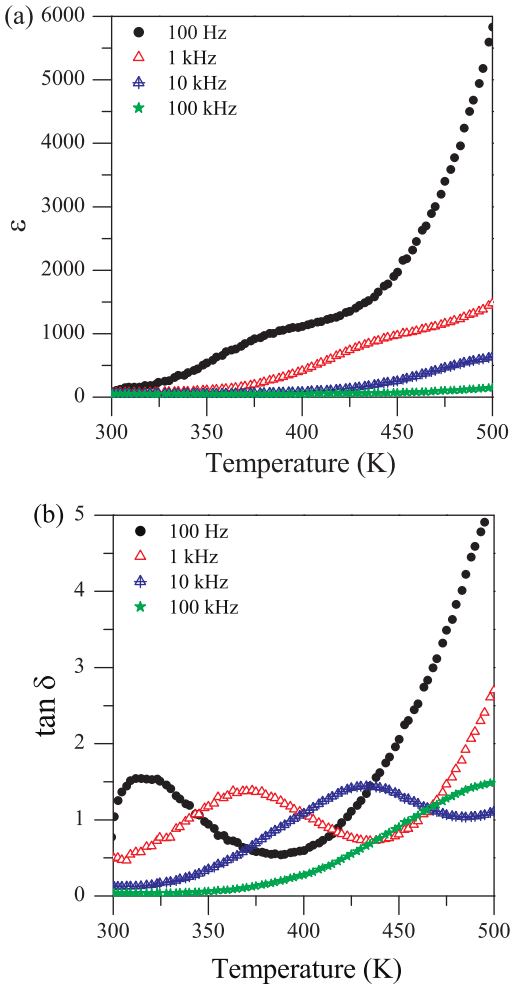

Fig. 3. Plots of: (a) dielectric constant (ε) and (b) dielectric loss ($\tan\delta$) vs temperature for $CaCu_{2.9}Fe_{0.1}Ti_4O_{12}$ (CCFTO) at selected frequencies.

frequency peak using the relation $\tau = 1/2\pi f$. Log τ vs. $1000/T$ plot is shown in Fig. 7. Linear nature of this plot shows that variation of τ with temperature can be expressed by the relation:

$$\tau = \tau_0 \exp\left(\frac{E_a}{kT}\right) \quad (1)$$

where E_a is the activation energy for dielectric relaxation and k is the Boltzmann constant. Value of E_a, determined by least square fitting of the data, is 0.42 eV. This value agrees with the value for Maxwell–Wagner polarization in the literature [10,24,25].

XPS measurements were carried out in order to determine the valence state of the cations. Figs. 8–10 show the high resolution core level XPS spectra of fractured surface of CCFTO sample. The O-1s spectra shown in Fig. 8, can be divided into two Gaussian bands with maxima at 529.2 eV and 531.1 eV. Similar results have been observed for CuO [26,27], $0.65Pb(Mg_{1/3}Nb_{2/3})O_3 - 0.35PbTiO_3$ single crystal [28] and thin films of $Ba_{0.5}Sr_{0.5}TiO_3$ [29]. Two peaks may correspond to two types of oxygen ions. The former can be attributed to the oxygen in the bulk while the latter can be ascribed to the chemisorbed oxygen [27]. Presence of an oxygen rich surface layer has been reported by Prakash and Varma [24].

The core level XPS spectra of Fe-2p and Ti-2p of the fractured surface of CCFTO are shown in Fig. 9(a and b), respectively. It can be seen from the Fig. 9(a) that the binding energies of $Fe2p_{3/2}$ and $Fe2p_{1/2}$ levels are 711.9 eV and 724.5 eV, respectively. This shows presence of iron as Fe^{3+} in CCFTO [30,31]. The satellite peak, associated with $Fe2p_{3/2}$ peak observed at 718.5 eV, is quite distinct.

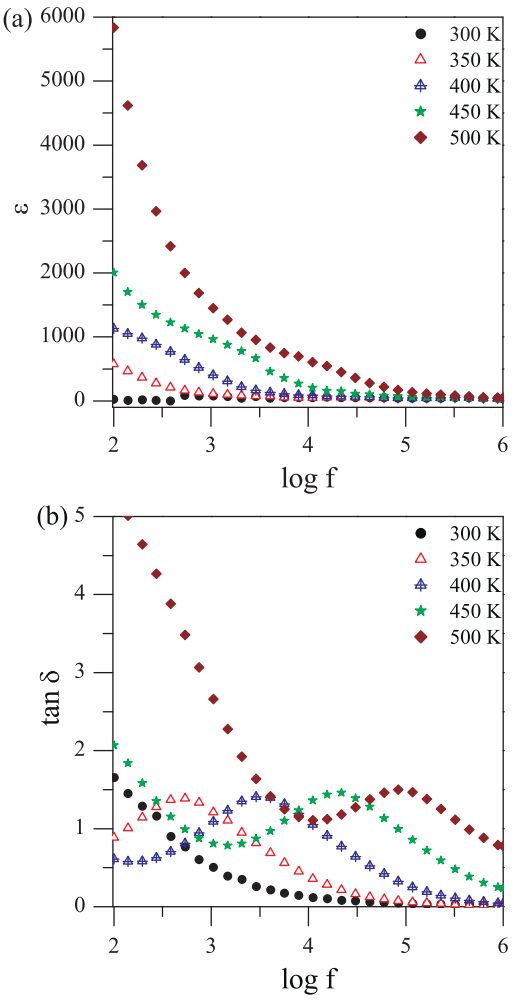

Fig. 4. Plots of: (a) dielectric constant (ε) and (b) dielectric loss (tan δ) vs log frequency for $CaCu_{2.9}Fe_{0.1}Ti_4O_{12}$ (CCFTO) at selected temperatures.

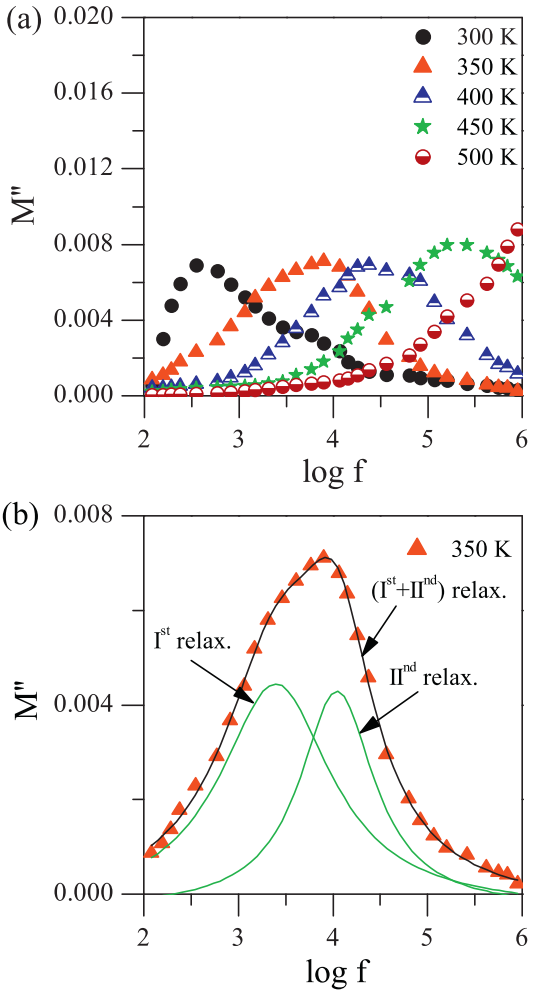

Fig. 6. (a) Plots of imaginary part of modulus (M'') vs. log f of $CaCu_{2.9}Fe_{0.1}Ti_4O_{12}$ (CCFTO) at different temperatures and (b) resolution of modulus spectroscopic plot at 350 K into two Gaussian curves.

Another satellite peak appears at 731.9 eV. This may be a satellite peak for Fe-$2p_{1/2}$. Fig. 9(b), demonstrates that Ti $2p_{3/2}$ and the Ti $2p_{1/2}$ core-level peaks are located at around 457.6 eV and 463.4 eV, respectively. These are very close to the experimental values reported for TiO_2 [32]. This shows that the Ti ions are in the tetravalent state i.e. there is no change in the valency of Ti^{4+} ions when Fe is doped on Cu site in CCTO.

Fig. 10(a and b) is plotted after correction of charging effects using a binding energy of 284.6 eV as C-1s peak. XPS shows Cu-$2p_{3/2}$ and Cu-$2p_{1/2}$ peaks at 933.5 eV and 953.6 eV, respectively in Fig. 10(a). Cu $2p_{3/2}$ spectra also have a satellite on the higher binding

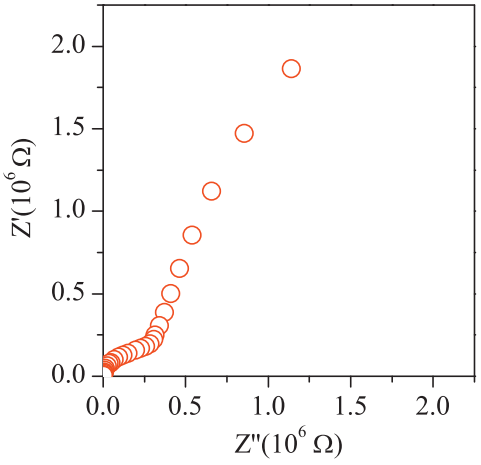

Fig. 5. Complex impedance plane plot of $CaCu_{2.9}Fe_{0.1}Ti_4O_{12}$ (CCFTO) at 400 K.

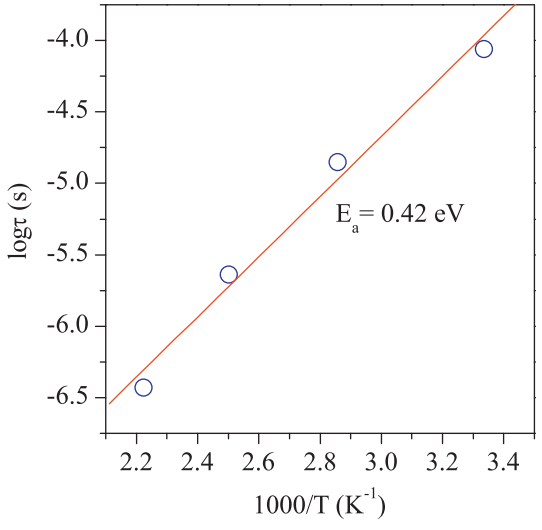

Fig. 7. Variation of relaxation time, τ with inverse of absolute temperature.

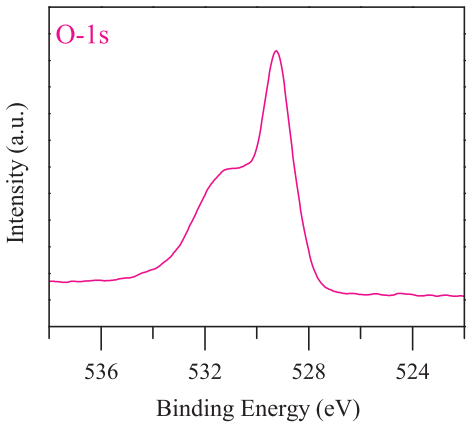

Fig. 8. X-ray photoelectron spectrum (XPS) of O-1s core level for CCFTO.

energy side which is similar to that reported for Cu^{2+} in CuO [33] or La–Sr–Cu and Y–Ba–Cu oxides [26]. The satellite peaks correspond to $2p3d^9$ configuration where 2p indicates that there is one electron missing (core hole) in the Cu-2p [34]. In a photoelectron emission process, electron charges are transferred from the surrounding to the core holes. Such a situation causes the main peak to be associated with a satellite at higher binding energy, as observed here [27]. The existing satellites confirm the existence of copper as Cu^{2+}. The satellite peak is absent in Cu_2O because it has a completely filled d shell (d^{10}). Fig. 10(b) shows two peaks at 345.8 eV and 349.4 eV corresponding to spin orbit doublets of Ca-$2p_{3/2}$ and Ca-$2p_{1/2}$, respectively. In CCTO, one shoulder which appears on higher energy side of each of these peaks has been ascribed to two different occupation sites of Ca ions [35], one site is in the CaO_{12} icosahedron and other is in the CuO_4 planar square. This result is similar to that observed in $Ba_{1-x}Ca_xTiO_3$. In $Ba_{1-x}Ca_x$ TiO_3 prepared by ceramic method, some of the Ca^{2+} occupies Ti^{4+} site inspite of a large difference in their size. This has been proved by Rietveld analysis [36].

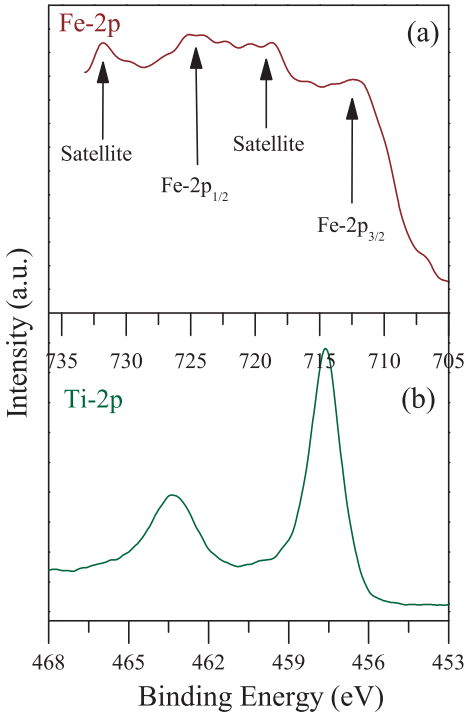

Fig. 9. X-ray photoelectron spectrum (XPS) of: (a) Fe-2p core level and (b) Ti-2p core level for CCFTO.

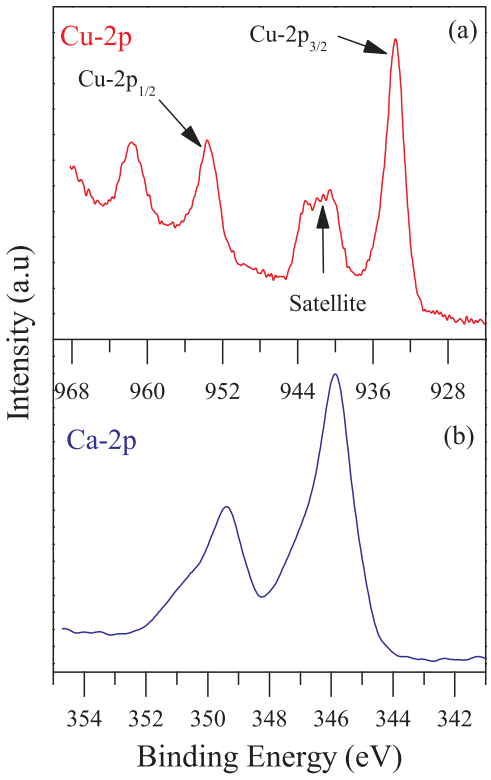

Fig. 10. X-ray photoelectron spectrum (XPS) of: (a) Cu-2p core level and (b) Ca-2p core level for CCFTO.

However, the shoulders are absent in CCFTO indicating that there is no disorder present on Ca and Cu site unlike in CCTO.

According to the above discussion, Ti^{4+} and Ca^{2+} show the same valency in CCFTO as in CCTO. Only some Cu^+ ions are oxidized to Cu^{2+} ions when Fe is doped in CCTO on the Cu sites. In CCTO, formation of Cu^+ ions may be explained simply by creation of oxygen vacancies which are produced due to loss of oxygen from the grains during sintering, as in most perovskite compounds [37]. The electrons produced in this process enter the 3d conduction band formed by the Cu atoms and not the Ti atoms as suggested earlier [38]. This gives rise to the formula $CaCu^{2+}_{3-x}Cu^{+}_{x}Ti_4O_{12-x/2}$. This can be expressed as follows:

$$O_o \leftrightarrow \tfrac{1}{2}O_2 + V_o^{\bullet\bullet} + 2e' \quad (2)$$

$$2Cu^{2+} + 2e' \rightarrow 2Cu^{+} \quad (3)$$

where all the species are written in accordance with Kröger Vink notation of defects. On substituting Fe^{2+} at Cu^{2+} site, formation of oxygen vacancies and Cu^+ ions is suppressed as under:

$$2(Cu^{+}_{Cu^{2+}})' + O_O + V_O^{\bullet\bullet} \xrightarrow{Fe_2O_3} 2Cu^{2+}_{Cu^{2+}} + 4O_O + 2Fe^{2+}_{Cu^{2+}} \quad (4)$$

A small concentration of iron exists in 2+ state while the major amount remains in 3+ state as indicated by XPS. It follows from the above discussion that substitution of iron at copper site suppresses disorder on Ca^{2+} and Cu^{2+} sites as well as presence of oxygen vacancies in the bulk. These factors which lead to high value of dielectric constant are absent in CCFTO. XPS results show that Cu^+ is oxidized to Cu^{2+} in CCFTO. This reduces oxygen vacancies through Eq. (4). The decrease in the number of oxygen vacancies will lead to an increase in the resistance of the bulk (grains) in CCFTO relative to CCTO. This has been evidenced by the impedance spectrum (Fig. 5(a)). This suggests that the permittivity in CCFTO ceramic can no longer be interpreted by the IBLC model. Absence of the IBLC mechanism is responsible for the drastic decrease in the permittivity of CCFTO as compared with that of CCTO. XPS studies show that

there is no disorder in CCFTO i.e. disorder at Ca/Cu sites is greatly suppressed when Fe is doped at Cu sites. Therefore, the suppression of disorder at Ca/Cu in CCFTO might be another reason for the greatly reduced permittivity.

4. Conclusions

Single phase CCFTO was successfully prepared using the powder synthesized by semi-wet route. Substitution of Fe^{3+} at Cu site in CCTO drastically reduces the dielectric constant. In CCFTO, XPS results suggest that Fe doped on Cu sites is present as Fe^{3+} and copper is present as Cu^{2+} in CCFTO. Traces of Fe may be in 2+ state. Both these factors will reduce the concentration of oxygen vacancies in the bulk CCFTO and lead to high resistivity of the grains. This suppresses the formation of IBLC layers at grains–grain boundaries. On the other hand, the disorder at Ca/Cu sites in CCFTO is suppressed. We conclude that substantial less value of permittivity of CCFTO than CCTO can be attributed to two reasons: one is the absence of the IBLC mechanism due to the increased resistivity of the grains in CCFTO and the other is the suppression of Ca/Cu disorder.

Acknowledgements

One of the authors "Alok Kumar Rai" would like to thanks to C. S. I. R, New Delhi, for award of Senior Research Fellowship (S. R. F.). This study was partially supported by a Priority Research Center Program and by the Basic Science Research Program of the National Research Foundation of Korea (NRF), funded by the Ministry of Education, Science and Technology (MEST) of the Korean government (2009-0094032 and 2010-0019694). Alok Kumar Rai is also thankful to the NRF's graduate research fellowship program (Post BK21) for financial support.

References

[1] A. Deschanvres, B. Raveau, F. Tollemer, Bull. Soc. Chem. Fr. 11 (1967) 4077.
[2] L. Fang, M. Shen, J. Yang, Z. Li, J. Phys. 38 (2005) 4236–4240.
[3] A.P. Ramirez, M.A. Subramanian, M. Gardel, G. Blumberg, D. Li, T. Vogt, S.M. Shapiro, Solid State Commun. 115 (2000) 217–220.
[4] P. Raevski, L. Jastrabic, J. Appl. Phys. 93 (2003) 4130–4136.
[5] A. Dixit, D. Maurya, D.P. Singh, D.C. Agrwal, Y.N. Mohapatra, Defence Sci. J. 57 (2007) 55–60.
[6] V. Brize, G. Gruener, J. Wolfman, K. Fatyeyeva, M. Tabellout, M. Gervais, F. Gervais, Mater. Sci. Eng. B 129 (2006) 135–138.
[7] Y. Zhu, J.C. Zheng, L. Wu, A.I. Frenkel, J. Hanson, P. Northrup, W. Ku, Phys. Rev. Lett. 99 (2007) 037602.
[8] M. Li, X.L. Chen, D.F. Zhang, W.Y. Wang, W.J. Wang, Sens. Actuators 147B (2010) 447–452.
[9] D. Capsonia, M. Binia, V. Massarotti, G. Chiodellib, M.C. Mozzatica, C.B. Azzonic, J. Solid State Chem. 177 (2004) 4494–4500.
[10] C. Mu, H. Zhang, Y. He, P. Liu, Physica B 405 (2010) 386–389.
[11] M. Li, A. Feteira, D.C. Sinclair, A.R. West, Appl. Phys. Lett. 88 (2006) 232903.
[12] J. Cai, Y.H. Lin, B. Cheng, C.W. Nan, J. He, Y. Wu, X. Chen, Appl. Phys. Lett. 91 (2007) 252905.
[13] W.C. Ribeiro, R.G.C. Araujo, P.R. Bueno, Appl. Phys. Lett. 98 (2011) 132906.
[14] L.F. Xu, P.B. Qi, X.P. Song, X.J. Luo, C.P. Yang, J. Alloys Compd. (2011) 105, doi:10.1016/j.jallcom.2011.02.
[15] W. Makcharoen, J. Tontrakoon, G. Rujijanagul, D.P. Cann, T. Tunkasiri, Ceram. Int. (2010) 051, doi:10.1016/j.ceramint.2011.04.
[16] A. Hassini, M. Gervais, J. Coulon, V.T. Phuoc, F. Gervais, Mater. Sci. Eng. B 87 (2001) 164–168.
[17] P. Jha, P. Arora, A.K. Ganguli, Mater. Lett. 57 (2003) 2443–2446.
[18] A.K. Rai, K.D. Mandal, D. Kumar, Om Parkash, Mater. Chem. Phys. 122. (2010) 217–223.
[19] A.K. Rai, K.D. Mandal, D. Kumar, Om Parkash, J. Alloys Compd. 491 (2010) 507–512.
[20] Z. Li, H. Fan, Solid State Ionics 192 (2011) 682–687.
[21] S. Ke, H. Huang, H. Fan, Appl. Phys. Lett. 89 (2006) 182904.
[22] R.K. Grubbs, E.L. Venturini, P.G. Ciem, J.J. Richardson, B.A. Tuttle, G.A. Samara, Phys. Rev. B 72 (2005) 104111.
[23] I.M. Hodge, M.D. Ingram, A.R. West, J. Electroanal. Chem. 74 (1976) 125–143.
[24] B.S. Prakash, K.B.R. Varma, J. Phys. Chem. Solids 68 (2007) 490–502.
[25] L. Zhang, Appl. Phys. Lett. 87 (2005) 022907.
[26] A. Fujimori, E. Takayama-Muromachi, Y. Uchida, B. Okai, Phys. Rev. B 35 (1987) 8814–8817.
[27] S. Sarkar, P.K. Jana, B.K. Chaudhuri, Appl. Phys. Lett. 89 (2006) 212905.
[28] Z. Xia, Q. Li, M. Cheng, Cryst. Res. Technol. 42 (5) (2007) 511–516.
[29] S.Y. Wang, B.L. Cheng, C. Wang, T.W. Button, S.Y. Dai, K.J. Jin, H.B. Lu, Y.L. Zhou, Z.H. Chen, G.Z. Yang, J. Phys. D: Appl. Phys. 39 (2006) 979–983.
[30] P.C.J. Graat, M.A.J. Somers, Appl. Surf. Sci. 100 (101) (1996) 36–40.
[31] S.J. Roosendaal, B. van Asselen, J.W. Elsenaar, A.M. Vredenberg, F.H.P.M. Habraken, Surf. Sci. 442 (1999) 329–337.
[32] R. Zimmermann, P. Steiner, R. Claessen, F. Reinert, S. Hufner, J. Electron. Spectrosc. Relat. Phenom. 96 (1998) 179.
[33] J. Ghijsen, L.H. Tjeng, J. Van Elp, H. Eskes, J. Westerink, G.A. Sawatzky, Phys. Rev. B 38 (1988) 11322–11330.
[34] Y.H. Lin, J. Cai, M. Li, C.W. Nan, J.L. He, Appl. Phys. Lett. 88 (2006) 172902.
[35] Z.H. Sun, C.H. Kim, H.B. Moon, Y.H. Jang, J.H. Cho, C.H. Song, Y.S. Yang, J. Korean Phys. Soc. 54 (2009) 881–885.
[36] P.S.R. Krishna, D. Pandey, V.S. Tiwari, R. Chakravarthy, B.A. Dasannacharya, Appl. Phys. Lett. 62 (1993) 231–233.
[37] F.D. Morrison, D.C. Sinclair, A.R. West, J. Am. Ceram. Soc. 84 (2001) 474–476.
[38] L. Zhang, Z.J. Tang, Phys. Rev. B 70 (2004) 174306.